Molecules and Cells

Characterizing Organelles in Live Stem Cells Using Label-Free Optical Diffraction Tomography

Youngkyu Kim[1], Tae-Keun Kim[1], Yeonhee Shin[2], Eunyoung Tak[1,2], Gi-Won Song[3], Yeon-Mok Oh[4], Jun Ki Kim[1,2,*], and Chan-Gi Pack[1,2,*]

[1]Asan Institute for Life Sciences, Asan Medical Center, Seoul 05505, Korea, [2]Department of Convergence Medicine, University of Ulsan College of Medicine, Seoul 05505, Korea, [3]Division of Hepatobiliary Surgery and Liver Transplantation, Department of Surgery, Asan Medical Center, University of Ulsan College of Medicine, Seoul 05505, Korea, [4]Department of Pulmonary and Critical Care Medicine, Clinical Research Center for Chronic Obstructive Airway Diseases, Asan Medical Center, University of Ulsan College of Medicine, Seoul 05505, Korea
*Correspondence: kim@amc.seoul.kr (JKK); changipack@amc.seoul.kr (CGP)
https://doi.org/10.14348/molcells.2021.0190
www.molcells.org

Label-free optical diffraction tomography (ODT), an imaging technology that does not require fluorescent labeling or other pre-processing, can overcome the limitations of conventional cell imaging technologies, such as fluorescence and electron microscopy. In this study, we used ODT to characterize the cellular organelles of three different stem cells—namely, human liver derived stem cell, human umbilical cord matrix derived mesenchymal stem cell, and human induced pluripotent stem cell—based on their refractive index and volume of organelles. The physical property of each stem cell was compared with that of fibroblast. Based on our findings, the characteristic physical properties of specific stem cells can be quantitatively distinguished based on their refractive index and volume of cellular organelles. Altogether, the method employed herein could aid in the distinction of living stem cells from normal cells without the use of fluorescence or specific biomarkers.

Keywords: high density vesicle, human stem cell, optical diffraction tomography, organelle volume, three-dimensional quantification

INTRODUCTION

In the last decade, stem cell research and therapy have been receiving attention in the field of translational research. Owing to the advances in stem cell research, the possibility of success in stem cell-based regenerative medicine and tissue engineering has been increasing. Stem cells are composed of organelles, similar to other cells. Organelles are divided into special subunits that are composed of cells and possess or not their own lipid bilayer (i.e., membrane bound or non-membrane bound organelles). These organelles are mainly nucleolus, ribosome, endoplasmic reticulum, Golgi apparatus, mitochondria, and various vesicles. In the field of cell biology and medicine, studying the interactions and properties of organelles is important as the findings allow us to understand the role and physiology of specific cells (Boulon et al., 2010; Németh and Grummt, 2018). Therefore, many studies have been conducted to image cell organelles using various microscopic techniques (Hantke et al., 2014; Wang and Hu, 2012; Zhu et al., 2016). For stem cells, many studies have only relied on detecting specific biomarkers rather than systematically imaging organelles or evaluating the morphological characteristics of organelles. Existing conventional bright-field microscopes mainly image the projection of the

Received 16 July, 2021; revised 27 August, 2021; accepted 9 September, 2021; published online 17 November, 2021

eISSN: 0219-1032

transmitted sample and provide morphological information based on two-dimensional images. As a result, it is difficult to accurately represent organelles owing to the low contrast of these images. Several types of imaging techniques have been developed to image organelles and overcome the disadvantage of general optical microscopes. Electron microscopes (EM) can image cell structure at ultra-high magnification using a metal or carbon coating on the outside of the cell depending on the application (Koster and Klumperman, 2003). With fluorescence microscopes, such as confocal laser scanning microscope (CLSM), the cell structure can be clearly confirmed by staining to generate a specific fluorescent signal in only target organelles of the cell sample. EM and CLSM enable the acquisition of images of cell structures in high resolution (Pepperkok and Ellenberg, 2006). However, EM requires metal or carbon coating, and these coatings make live cell imaging difficult. Fluorescence microscopy needs additional cell treatment, such as gene modification for expressing fluorescent protein or staining fluorescence dye, even though it is applicable to both living cells and fixed cells. These additional cell treatment and preparation steps are markedly time- and labor-consuming processes and might cause unwanted effects by affecting cell physiology, such as inducing cellular phototoxicity (Magidson and Khodjakov, 2013).

Optical diffraction tomography (ODT), an imaging technology that does not require fluorescent labeling or other pre-processing, can overcome the limitations of former cell imaging technology (Park et al., 2008; Wolf, 1969). ODT is one of the non-invasive quantitative phase imaging (QPI) technologies that is now widely used in biology and medicine (Kim et al., 2016a; 2018c; Li et al., 2019; Stanly et al., 2020). Using digital holographic information and backlight scattering principle, ODT reconstructs the phase difference image of cells at high speed and provides the three-dimensional (3D) refractive index (RI) and volume information of living cells as well as fixed cells. If there is a clear difference in the shape and RI of each organelle, it is predicted that it can be detected using ODT. For example, recent previous studies have demonstrated that the nuclear membrane and nucleoli of live HeLa cells and the chromosomes of Indian Muntjac fibroblast cells during cell division can be imaged and characterized based on the RI (Kim et al., 2019a; 2019b). However, the extent to which various organelles existing in cells can be distinguished using ODT remains unclear (Gnutt et al., 2015; Johnsen and Widder, 1999; Sawyer et al., 2019). Nonetheless, ODT is a non-labeled technology that does not provide molecular-related information. Instead, images are constructed by distinguishing different RI values, and this spproach does not always automatically separate specific cellular structures.

In this study, we used a label-free ODT technique to characterize three different types of stem cells and one fibroblast cell. First, we used human liver derived stem cells (hLD-SC), which differ from hepatic progenitor cells, possess mesenchymal stem cell (MSC)-like characteristics, including differentiation ability and immunosuppressive effect, and are negative for the hematopoietic stem cell marker, CD34 (Herrera et al., 2006; Najimi et al., 2007; Pan et al., 2011). Second, we used human umbilical cord matrix derived mesenchymal stem cells (hUCM-MSC) which are undifferentiated multipotent non-hematopoietic stem cells that are capable of self-renewal and differentiation into many cell types; these cells are used in various drug discovery and cell therapy investigations (Choi et al., 2014). Finally, we used human induced pluripotent stem cells (hiPSC). Although these stem cells are expected to be widely applied in clinical cell therapy, it is still unclear how the physical properties of stem cells differ and their distinctive characteristics from cells without self-renewal function. These three types of stem cells were compared with fibroblast to evaluate the RI and volume of the nucleoli and vesicles with high RI. It is important to evaluate cell characteristics under various physiological conditions (Lee et al., 2012; 2020; Pan et al., 2011). Using conventional microscope techniques, confirmation of the expression of various biomarkers (i.e., immunofluorescent or immune-gold observation) are typical methods and two-dimensional evaluation using fixed cells. However, such methods are phototoxic and invasive, which limit their ability to be used to precisely determine the characteristic property of each organelles of cells.

Our findings demonstrate that ODT can be used to image stem cells and quantify the nucleoli and vesicular structures according to cell type based on RI and volume. Interestingly, the RI of the vesicular structure distributed in each stem cell was markedly higher than that distributed in fibroblast cells. Moreover, through a comparison of electron microscopic and ODT analyses, we found that unlike in fibroblast cells, the large volume of vesicles distributed in stem cells had a high density. These results demonstrate that the characteristics of specific stem cells can be quantitatively distinguished based on the RI and volume of cellular organelles and thus can be used to distinguish living stem cells from normal cells without the use of fluorescence or specific biomarkers.

MATERIALS AND METHODS

Ethics and governance

The study was conducted in accordance with the guidelines of the Declaration of Helsinki, and all study protocols were reviewed and approved by the Institutional Review Board (IRB) of Asan Medical Center (Korea). For hLD-SC, consent was obtained from a liver donor who visited the Division of Liver Transplantation and Hepatobiliary Surgery (IRB protocol No. 2018-1386). hUCM-MSC was donated from a full-term baby who visited Asan Medical Center (IRB protocol No. 2015-3030). For skin fibroblasts, informed consent was obtained from participants who visited the Department of Pediatrics at Asan Medical Center (IRB protocol No. 2017-0260). All established stem cell lines were registered and are managed by the Stem Cell Center at Asan Institute of Life Science, Asan Medical Center. The current study was conducted using anonymized stem cell lines from the Stem Cell Center.

Preparation of human stem cells and cell culture

hLD-SCs were derived from human liver and cultured in Dulbecco's modified Eagle medium: Nutrient Mixture F-12 (DMEM/F-12) supplemented with 10% fetal bovine serum (FBS), 100 U/ml penicillin, and 100 U/ml streptomycin at 37°C in an atmosphere containing 5% CO_2 (Lee et al., 2020).

hUCM-MSCs were derived from human umbilical cord matrix and cultured in DMEM/F-12 supplemented with 10% FBS, 100 U/ml penicillin, and 100 U/ml streptomycin at 37°C in an atmosphere containing 5% CO_2 (Kim et al., 2018b). hiPSCs were derived from peripheral blood mononuclear cells (PBMCs) and cultured in StemMACS supplemented with 100 U/ml penicillin and 100 U/ml streptomycin at 37°C in an atmosphere containing 5% CO_2 (So et al., 2020). Fibroblasts were derived from human skin and cultured in DMEM/F-12 supplemented with 10% FBS, 100 U/ml penicillin, and 100 U/ml streptomycin at 37°C in an atmosphere containing 5% CO_2 (Lee et al., 2021). For live cell microscopy, stem cells and fibroblasts were plated in Tomo-dishes (Tomocube, Korea)

Transmission electron microscopy

For transmission electron microscopy (TEM) imaging, we used a modified TEM method (Jung et al., 2020; Woo et al., 2021). Each stem cell was grown in 100 mm culture dishes to 70%-80% confluency. Cells were fixed with 1% paraformaldehyde (Tech and Innovation, Korea) and 1% glutaraldehyde (EMS, USA) diluted in 0.1 M sodium cacodylate buffer. After the cells were washed and post-fixed in 2% osmium tetroxide (OsO_4) for 1 h at 4°C, they were dehydrated using an ethanol series (70%, 80%, 90%, 95%, and 100%) for 30 min at each concentration. The samples were then embedded with an epoxy resin embedding kit (Ted Pella, USA). The embedded samples were then sectioned (60 nm) with an ultramicrotome (Leica, Germany) and mounted on copper 200 mesh grids with a specimen. Thereafter, they were double-stained with 2.5% uranyl acetate in 50% Acetone for 16 min and lead citrate for 7 min. The specimens were viewed under a transmission EM at 80 kV (Hitachi H-7600, Hitachi, Japan).

Label-free ODT

ODT was performed as described previously (Kim et al., 2019a; Park et al., 2010). ODT reconstructs 3D RI tomography of a cell sample from multiple 2D hologram images of the sample acquired at various angles (Kim et al., 2018a). ODT measurement of single living cells was performed with a commercial ODT microscope (HT-2H; Tomocube) using a 532 nm laser light source at 37°C in an atmosphere containing 5% CO_2 (Jung et al., 2016; Kim et al., 2018c; 2019a; Park et al., 2010). The commercial ODT microscope which is based

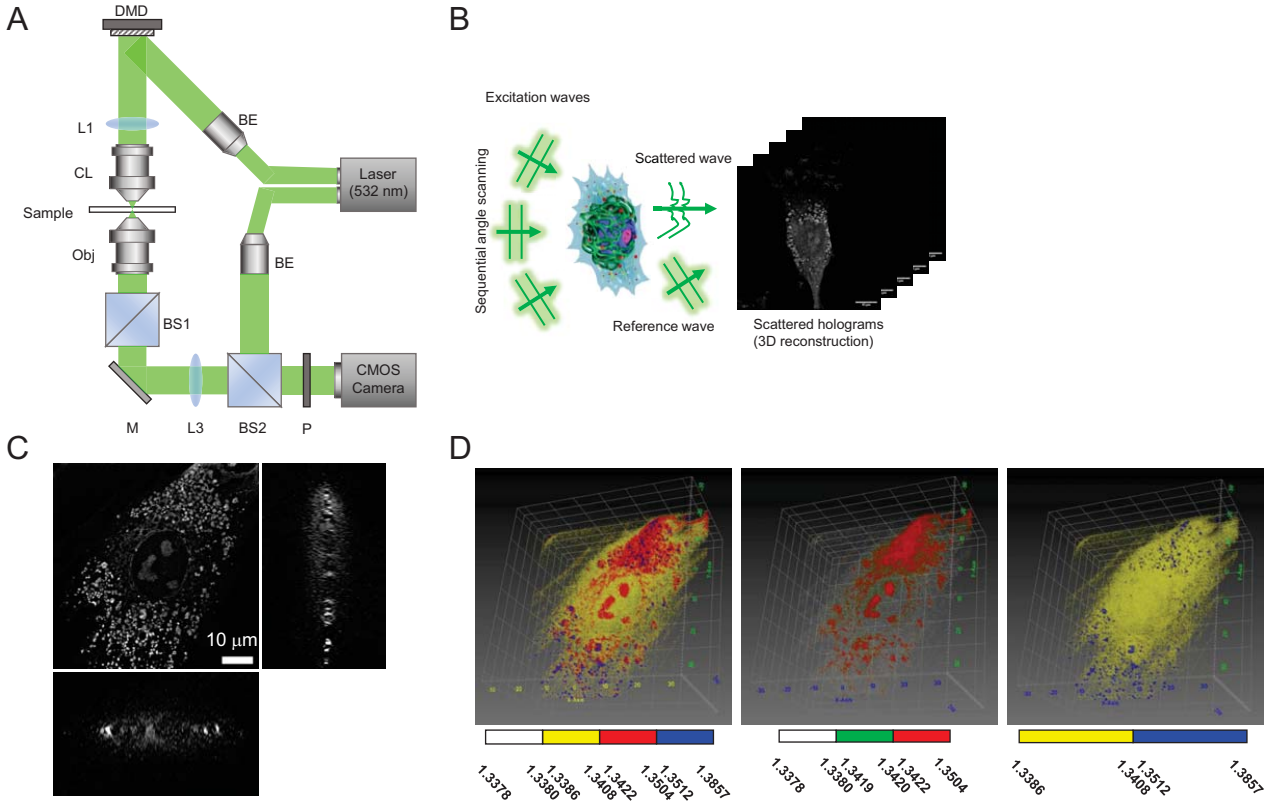

Fig. 1. Schematic of a label-free 3D ODT setup and image generation. (A) Optical system setup for optical diffraction tomography. BE, beam expander; CL, condenser lens; Obj, objective lens; M, mirror; BS, beam splitter; P, polarizer; CMOS, complementary metal-oxide-semiconductor. (B) Conceptual diagram of three-dimensional reconstruction by acquiring a 2D hologram image using scattered and reference light to generate phase change and intensity change while the excitation light in multiple directions incident on a transparent cell passes through the cell. (C) Cross-sectional slices of the 3D image in the x-y, x-z, and y-z planes of a hUCM-MSC obtained using HT-2 ODT microscope. Scale bar = 10 μm. (D) RI rendered image obtained by mapping the RI based on the image shown in (C). The RI ranges used for RI rendering are depicted by pseudo color bars.

on Mach-Zehnder interferometry equipped with a digital micromirror device (DMD) to reconstruct the 3D RI tomography of cells. The DMD was used to control the angle of an illumination beam impinging onto the sample. The ODT system has 0.05 mW laser power, 110 nm lateral resolution, 356 nm axial resolution and 2.5 fps at 3D image acquisition specifcations (Park et al., 2018). Details of the optical setup for the ODT system are described in Fig. 1. Briefly, the microscope was composed of a light source/sample modulation device and an optical field detector device. Optical interfer-

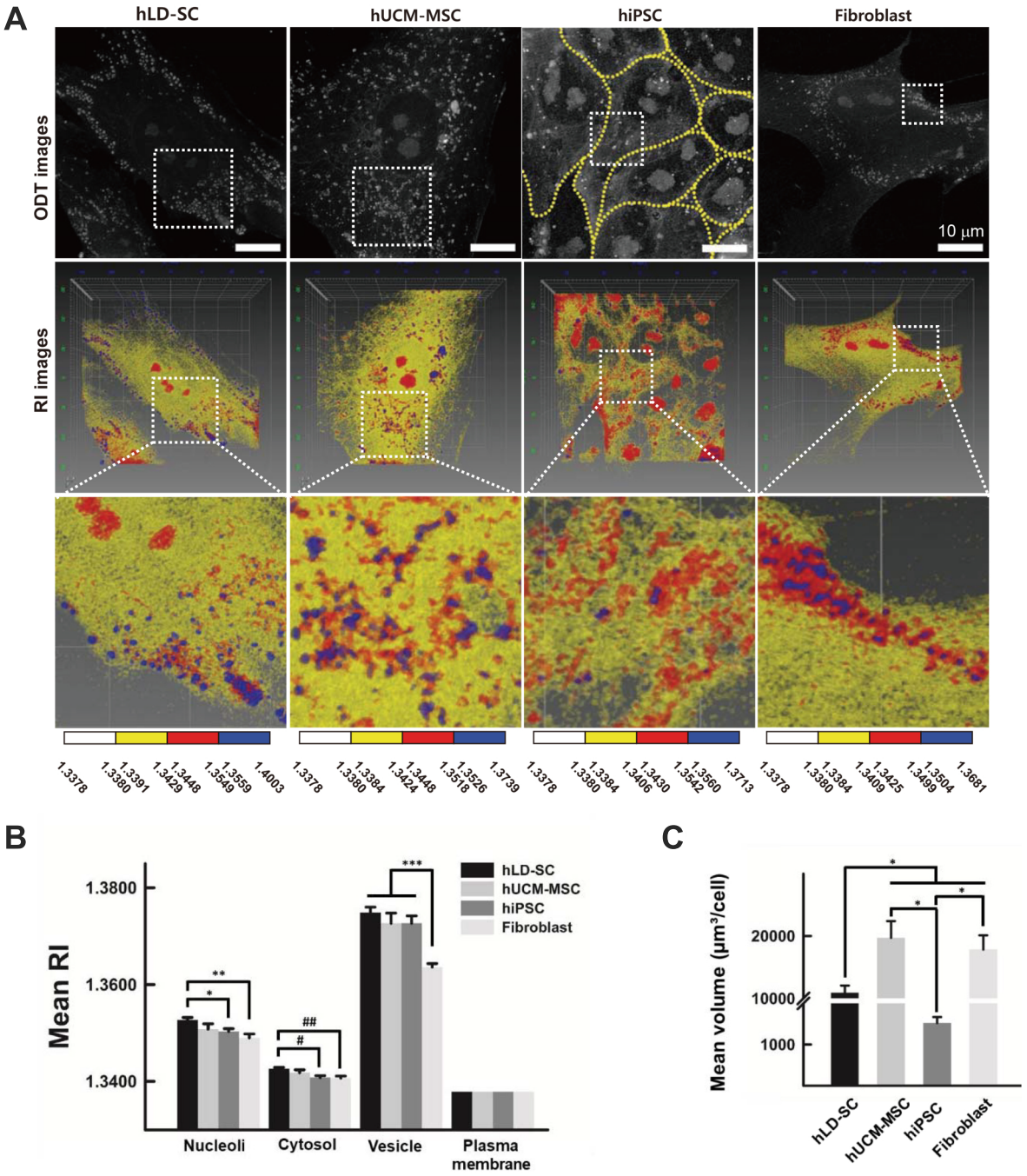

Fig. 2. Label-free 3D ODT image acquisition and quantitative analysis of RI and cell volume for three different stem cells and fibroblasts. (A) Representative raw ODT image for hLD-SC, hUCM-MSC, hiPSC, and fibroblast (top), RI mapping image for each cell (center), enlarged RI mapping image for the dense part of the vesicular structure (bottom, blue). The RI ranges used for RI rendering are depicted by color bars. Scale bars = 10 μm. (B) Mean RI values for organelles (nucleoli, cytoplasm, vesicles, plasma membrane) of each cell (n = 20 cells). (C) Mean volumes of a cell for each cell type (n = 20 cells). $*P < 0.005$, $**P < 0.0005$, $***P < 0.0005$, $^{\#}P < 0.005$, $^{\#\#}P < 0.0001$.

ence was used to record the amplitude and phase information from light passing through a cell sample. The RI value of each plasma membrane was used as a reference point to measure ODT cells (Kim et al., 2019a; 2019b). Adjustment of the power and exposure time of the laser projected onto the sample cells was first performed to ensure that it did not negatively affect the RI value measurement or image quality; these parameters were then fixed during the ODT measurement. The RI value of each culture medium was used as reference for ODT cell measurement. To verify the capability of the system, microspheres with a diameter of 6 μm (Polysciences Inc., USA) were used (Kim et al., 2019b). The lateral and axial optical resolutions of the ODT system were 200 nm and 1 μm. The resolution of the RI value is <0.001 (Kim et al., 2018a; 2019a).

Image rendering and evaluation of RI and cell volume

The RI iso-surface of the cytoplasm, nucleolus, and vesicle of the cell was rendered using TomoStudio software (2.6.25; Tomocube) according to the manufacturer's protocol (Kim et al., 2019a; 2019b). RI values were also calculated using this software (see also Supplementary Fig. S1). User-defined transfer functions representing various RI values and the range of the RI gradient sizes were altered using TomoStudio's virtual palette until 3D rendered images of plasma membrane, cytoplasm, vesicle, and nucleolus were sufficiently explained compared to the reference. The median value of the RI range was used to calculate the mean RI values for the cytoplasm, nucleolus, and vesicle of each cell in each medium condition.

Surface volume calculation

RI images acquired using ODT were 3D rendered using IMARIS 8.1.2 software (Bitplane, USA) and used for vesicle and nucleolus count and volume analysis (see also Supplementary Fig. S1). Before using IMARIS software for 3D rendering, we extracted each specific organelle image from the ODT RI raw images using MATLAB (Mathworks, USA) and their RI values. The surface function of the IMARIS software was used for the number and volume analysis of these organelles.

Statistical methods

Student's *t*-tests were performed to compare the mean values and determine significance (Origin v.8.5; OriginLab, USA). All *P* values less than 0.05 were considered significant.

RESULTS

Acquisition of label-free 3D ODT image and quantification of the RI of organelles

Information regarding the ODT instrument used in this study is presented in Fig. 1A. Multiple 2D holograms of the sample were acquired at various illumination angles via a Mach–Zehnder interferometric microscope equipped with a DMD. The scattered beam wave of the sample interfered with the tile reference beam wave and produced a spatially modulated hologram (Fig. 1B). Phase images scattered from the recorded holograms, amplitudes, and samples were obtained using a phase search algorithm (Debnath and Park, 2011; Takeda et al., 1982). Based on the algorithm, label-free ODT produces an RI distribution by assembling the RI range of images acquired from sequential angles scanned from two-dimensional holograms. 3D RI tomography of the sample was reconstructed from several 2D holograms as shown in Figs. 1C and 1D (see also Supplementary Fig. S1).

Label-free 3D ODT images were obtained from each stem cell (hLD-SC, hUCM-MSC, and hiPSC), and fibroblast (Fig. 2A, Supplementary Fig. S1, Supplementary Movies S1-S4). Using raw ODT images, the RI mapping image was reconstructed by dividing the corresponding RI ranges of the nucleolus, cytoplasm, vesicles, and plasma membrane for each cell type. Although the cell membrane, cytoplasm, and nucleolus could be identified morphologically, the vesicular structure with a high RI and small size observed in the cytoplasm was not clear. As a result, it was classified as a vesicle for simplicity. Figure 2B summarizes the mean RI values of the nucleolus, cytoplasm, vesicles, and plasma membrane, which were derived from the rendered RI images (see Materials and Methods section). The cell plasma membrane of each cell is expressed by the same RI value. In contrast, the mean RI values of hLD-SC nucleoli were significantly different from those of hiPSCs and fibroblasts. Similar differences were also found in the cytoplasm. Interestingly, the RI values of the vesicular structure (vesicle) of hLD-SC, hUCM-MSC, and hiPSC were markedly larger than that of fibroblast, suggesting that many vesicles distributed in cells may be characteristic of stem cells only. The RI value of a sample (i.e., organelle) is proportional to the molecular density contained in the sample due to the relationship of $n = n_0 + \alpha c$, where n and n_0 indicate the RI values of the sample and the surrounding medium, respectively, and α and c indicate the RI increment and the concentration of biomolecules, respectively (Barer, 1953; Popescu et al.,

Table 1. Calculated mean molecular density of the cellular organelles

Cellular component	Molecular density (g/ml)			
	hLD-SC	hUCM-MSC	hiPSC	Fibroblast
Nucleolus	0.0950 ± 0.0027	0.0854 ± 0.0057	0.0828 ± 0.0030	0.0763 ± 0.0039
Cytosol	0.0447 ± 0.0013	0.0404 ± 0.0029	0.0357 ± 0.0018	0.0349 ± 0.0018
Vesicle	0.2059 ± 0.0058	0.1948 ± 0.0109	0.1949 ± 0.0077	0.1495 ± 0.0038
Plasma membrane	0.0210	0.0210	0.0210	0.0210

Values are presented as mean ± SD.
Molecular density was caculated using the refractive index increment α = 0.2 ml/g for protein.
The molecular density (i.e., RI value) of the plasma membrane did not differ according to the cells.

2008; Yoon et al., 2017). Therefore, if the RI value is evaluated from the ODT measurement, the molecular density of the biomolecules contained in the sample can be estimated. The RI increment α depends on the sample type, light source wavelength, and temperature. However, proteins have a mean α value of 0.2 ml/g, when a light source of 532 nm is employed (Yoon et al., 2017). For the comparison of RI and molecular density, Table 1 summarizes the protein molecular density for each organelle calculated using the average RI value obtained with ODT. Figure 2C shows the mean volume of a

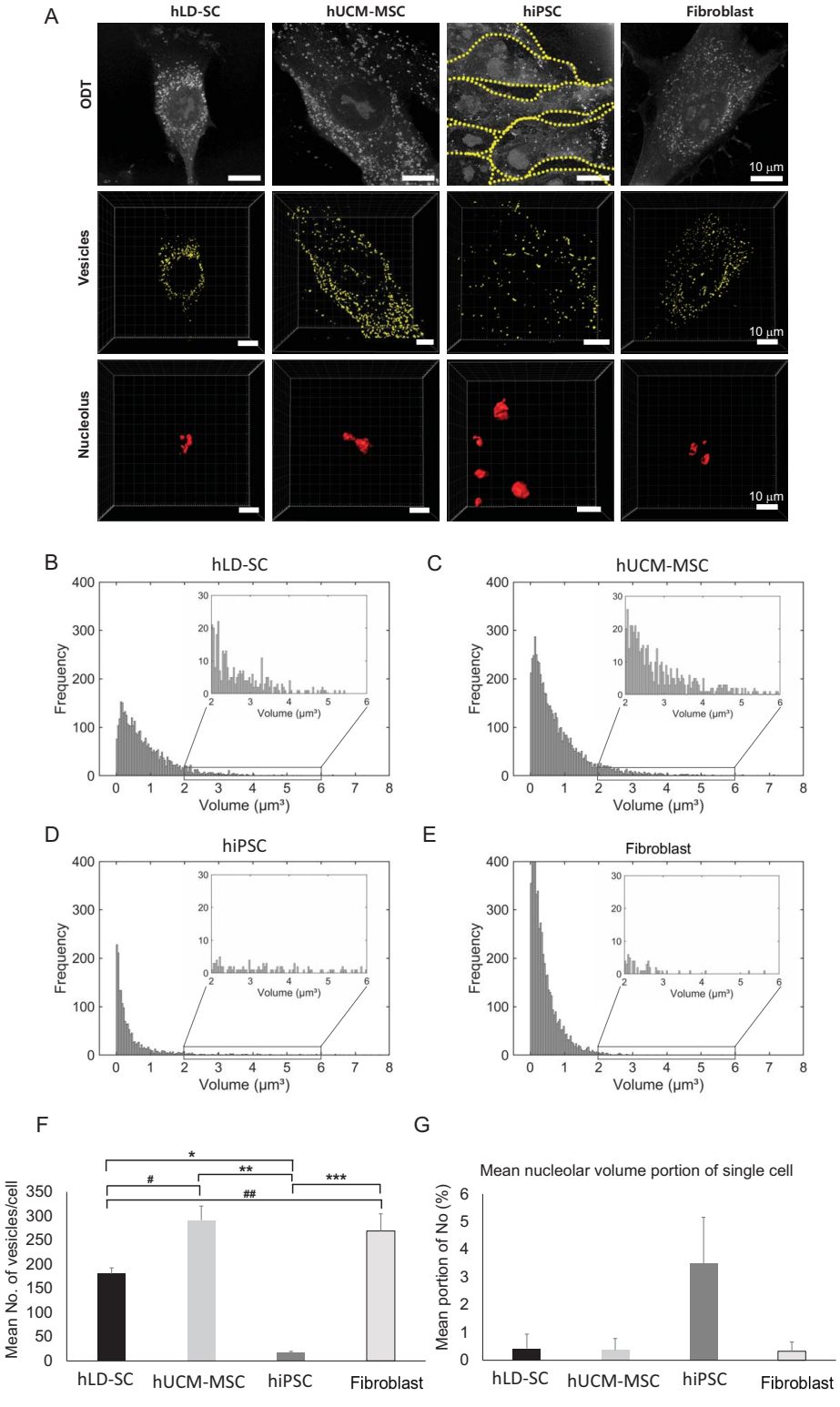

Fig. 3. The number and volume of the vesicular structures and nucleoli using label-free 3D ODT images. (A) Representative 3D ODT images of hLD-SC, hUCM-MSC, hiPSC, and fibroblast (top). 3D Images of the vesicular structure (center) and the nucleolus (bottom) detected in each cell were extracted and reconstructed for numerical and volumetric analysis. (B-E) Histograms of the volume of single vesicles found in the four cell types (cell number, n = 20 cells). For clarity, a portion of large volume areas from 2 to 6 μm^3 was enlarged (inset). (F) Mean number of the vesicle found in a single cell. $*P < 0.0001$, $**P < 0.0001$, $***P < 0.0001$, $^{\#}P < 0.001$, $^{\#\#}P < 0.05$. (G) Mean nucleolar volume portion (volume of the nucleolus/volume of a cell) of a single cell. No, nucleolus.

single cell for each cell type. For hiPSC, the volume evaluation of the cells was slightly unreliable as these cells proliferated by forming colonies. Fortunately, as the nucleolus and the cytoplasm of the cell can be clearly distinguished, the number of cells was determined based on this and the average volume was calculated by dividing the total colony volume by the number of cells. In contrast to hiPSC, for all other cell types, only single cells were clearly distinguished and analyzed. The mean volume of single hiPSC was markedly smaller than that of other cell types. hUCM-MSC and fibroblast did not display any difference in single cell volume. However, the single cell volume of the hLD-SC was half that of the hUCM-MSC and fibroblast. These results indicate that cell volume is not a major characteristic of the two stem cells alone.

Volumetric and numerical analysis of the nucleoli and vesicles

As the mean RI of the nucleoli and vesicular structures (i.e., vesicles) was higher for stem cells than fibroblasts, the volume and number of the organelles in a single cell were respectively analyzed to determine the volumetric and numeric characteristics of the organelles. Label-free ODT images of three different stem cells and fibroblasts were used to reconstruct 3D images of the vesicles and nucleoli of each cell using IMARIS software (Fig. 3A, see also Supplementary Fig. S1). Based on the reconstructed 3D image of the organelles, both the volume and number of the two organelles were respectively evaluated. For hiPSC, the number of cells was first determined using the counted number of the nucleus as described. Thereafter, the mean volume of the nucleolus and mean number of the vesicle per single cell were calculated by dividing the total volume and number by the number of cells. As single-cell imaging was possible for hLD-SC, hUCM-MSC, and fibroblast, the volume and number of nucleoli and vesicles were calculated for each single cell in this case. Although the mean volume of single vesicles for stem cells was markedly larger than that of fibroblast, the median volume for all cell type had a value lower than the mean value (Table 2). This finding indicates that the distribution of volume of single vesicles is not a normal distribution, but a right-skewed distribution (Figs. 3B-3E). As shown in the histograms for the volume of single vesicles, hLD-SC and hUCM-MSC had a relatively large number of vesicles with a large volume compared to other cell types (inset). Quantitative analysis of the correlation between the single vesicle volume and RI is difficult with current analytical techniques using RI rendering. Nevertheless, as the mean RI value of hLD-SC, hiPSC, and hUCM-MSC vesicles was higher than that of the fibroblast vesicles and large-volume vesicles were widely distributed, these characteristics were considered to be possessed only by these three types of stem cells. However, hiPSC vesicles had fewer large-volume vesicles than the other two stem cells. Interestingly, the mean number of vesicles per hiPSC was markedly lower than that of other cell types (Fig. 3F). Furthermore, there is a characteristic for hiPSC that the ratio of the volume occupied by the nucleolus to the average volume of one cell is very large compared to that of other cell types (Fig. 3G).

Ultra-structural analysis using TEM

As shown in Figs. 1 and 3, vesicular structures with high RI and large volume were specifically observed in stem cells. Therefore, to confirm how specific vesicles distributed in living stem cells, as identified using ODT, differ from those of fibroblasts, the ultrastructure of intracellular vesicles was analyzed using TEM (Fig. 4). Although the two-dimensional TEM image obtained using fixed cells could not be directly compared with the three-dimensional image of living cells from ODT, it could suggest why there are differences in the physical properties of vesicles. As shown in Figs. 4A-4D, vesicles of various sizes were distributed within each cell. Interestingly, unlike fibroblasts, unknown structures with high electron density inside vesicles were often found in hLD-SCs and hUCM-MSCs (Figs. 4E-4G). Although the total number of vesicles in hiPSCs was very small compared to that in other cells (Fig. 3D), large vesicle filled with multiple vesicular structure was present, as found in other stem cells (Fig. 4H). However, for the nucleolus, it was difficult to distinguish a characteristic difference with 2-D TEM images, except that the nucleolus of hiPSC was significantly larger than that of other cell types (see also Fig. 3G).

DISCUSSION

As various undifferentiated stem cells, such as MSCs and iPSCs, differ in specific aspects, especially as biomarkers and in their biological functions, methods such as immunostaining for biomarker detection have been mainly used to confirm the biological properties of these cells (Al-Bagdadi et al., 2019; Manos et al., 2011). These conventional methods have invasive limitations as they require fixed cells or fluorescent- or immune-staining, which raises an essential question regarding the differences in characteristics of each living cell. ODT, which can be used to evaluate the physical properties of cells and organelles, is useful for non-invasive and spatio-temporal analysis of living cells, but does not provide biological information on the expression and function of specific biomarkers of stem cells. Nevertheless, if characteristics with different physical properties can be specifically defined between different cells, it will be possible to distinguish the types and characteristics of cells directly as living cells without the need for immunostaining or fixation. However, the physical properties of various organelles in stem cells are still unclear. In this study, the morphological and physical char-

Table 2. Summary of the mean and medial volume of single vesicles

	Volume of single vesicles (μm^3)			
	hLD-SC	hUCM-MSC	hiPSC	Fibroblast
Mean ± SD	0.8654 ± 0.0137	0.8307 ± 0.0119	1.0595 ± 0.1445	0.4272 ± 0.0059
Median	0.6357	0.5545	0.2366	0.2936

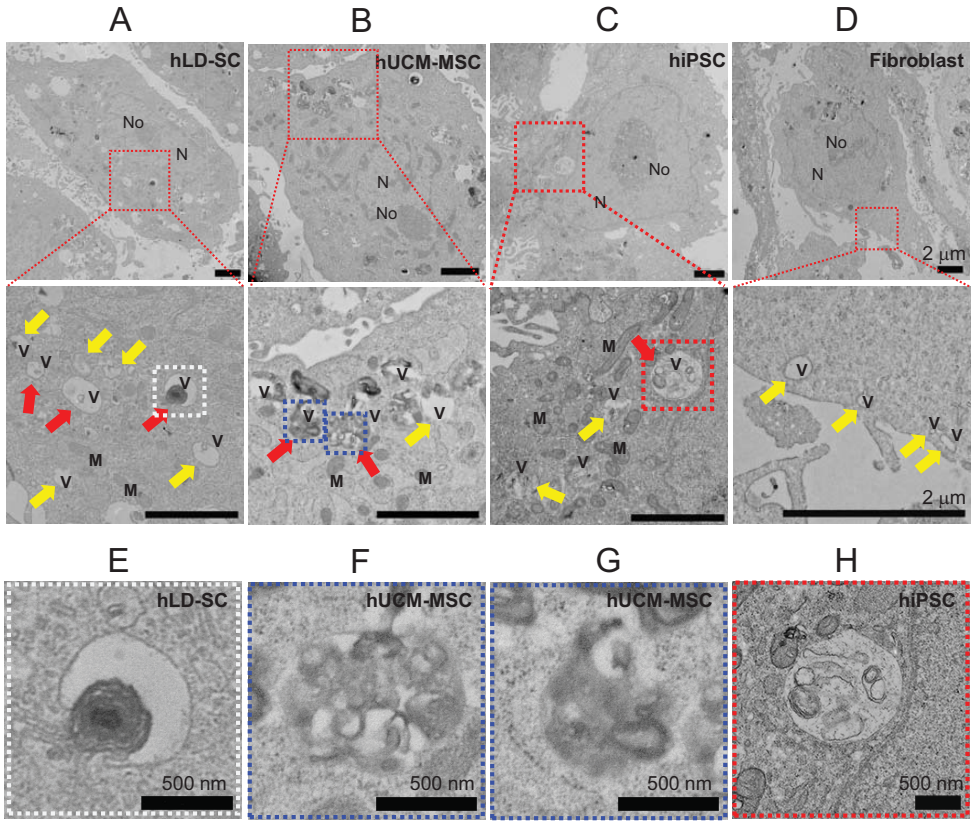

Fig. 4. Ultrastructural analysis of organelles using TEM. Representative TEM images for hLD-SC (A), hUCM-MSC (B), hiPSC (C), and fibroblast (D). N, nucleus; No, nucleolus; M, mitochondria; V, vesicle (upper). Scale bars = 2 μm. An enlarged image of the region containing vesicles in each cell (red) is shown (lower). Scale bars = 2 μm. Yellow and red arrows indicate hollow vesicles and vesicles with unknown dense structures inside the vesicles, respectively. (E-H) Enlarged TEM images of large and dense vesicular structure appearing in hLD-SC (white), hUCM-MSC (blue), and hiPSC (red) as shown in (A-C) are shown. Scale bars = 500 nm.

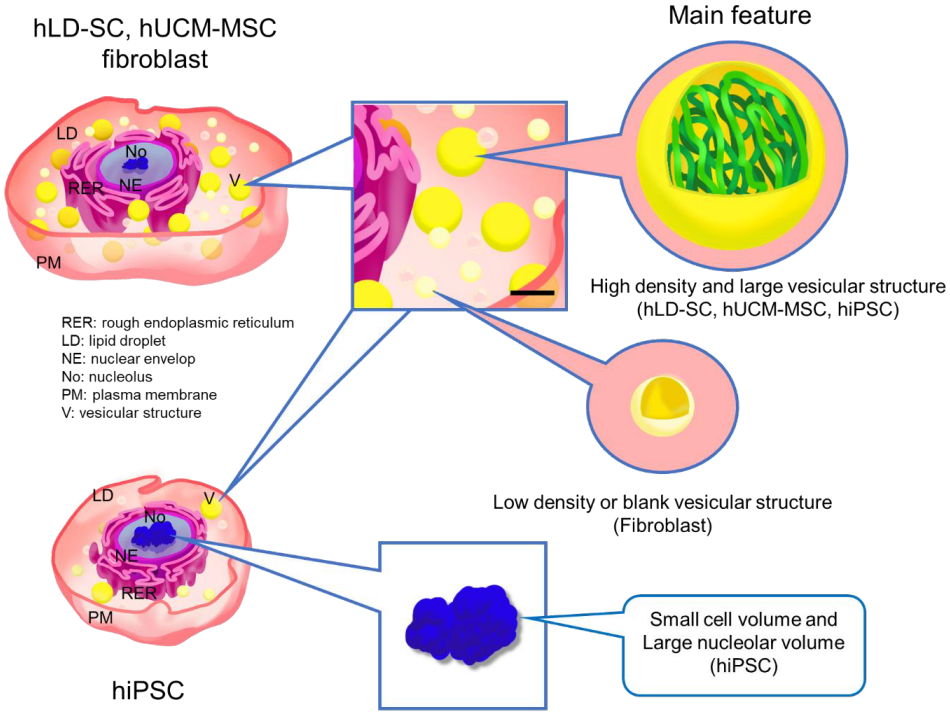

Fig. 5. Schematic showing the unique physical properties of the vesicle and nucleolus found in stem cells. Compared to fibroblasts, hiPSC, hLD-SC, and hUCM-MSC have relatively large volume and dense vesicle distribution, even though the number of vesicles contained in a single cell varies from cell to cell (top). In addition to these characteristic vesiclular structure, hiPSCs are characterized by a relatively small cell volume and a large nucleolus (bottom). Scale bar = 1 μm.

acteristics of two stem cells of different origins, iPSCs, and fibroblast cells were analyzed and compared for the first time using label-free and non-invasive ODT, which is one of the well-established QPI techniques.

ODT analysis on live cells revealed that the molecular density of the cytoplasm and the nucleolus in LD-SC cells were significantly higher than those of hiPSC and fibroblast cells. Interestingly, the mean RI of the vesicles distributed in the three stem cells was markedly higher than that in the fibroblast cells. Moreover, when the vesicles were compared, hLD-SC, hUCM-MSC, and hiPSC were found to contain many vesicles with a markedly larger volume than fibroblast cells. Similarly, it was suggested that large vesicles containing specific rounded structures with high electron density were often found in the hLD-SC, hUCM-MSC, and hiPSC using TEM analyses. The identity of the rounded and highly dense structure remains unclear. However, the density of the vesicles might increase and the volume may also increase owing to this dense content. Various vesicle organelles formed in a single membrane, such as lysosome, endosome, and lipid droplet (LD), exist in the cell. As various stem cells produce a large amount of exosomes, the multivesicular body required to generate these exosomes in stem cells can be distributed more than that in other cells. Nevertheless, these vesicles with rounded structure and large size are thought to be related to the high average RI and large volume distribution revealed by the ODT analysis. A previous study using ODT reported that the volume of LD distributed in cultured cells (hepatocytes) was approximately 0.47 μm^3, and there were approximately 150 LDs per cell (Kim et al., 2016b). In addition, it is suggested that the mean RI of these LDs is approximately 1.385. Owing to an analysis of LD using HeLa cells, it was confirmed that they had approximately the same RI value (Supplementary Fig. S2). The RI value of LD is markedly larger than those of vesicular structures found in stem cells and fibroblast cells. Therefore, the vesicles seen in these stem cells and fibroblast cells are considered to be vesicle organelles other than LD. The number of vesicles per unit cell for hiPSC is very small compared to other cells, and the volume ratio of the nucleolus is very large compared to other cells. Therefore, hiPSC can be easily distinguished from the other three types of cells. The various organelles present in the cell may dynamically change in quantity and quality according to the cell cycle. Recently, in a previous study, the density of various compartments such as the cytoplasm, nucleoplasm, and nucleolus of a cell was maintained constant during cell growth (i.e., the cell cycle), whereas the volume of each compartment was maintained by depolymerization of actin and microtuble or chromatin condensation, shape, and dry mass change (Kim and Guck, 2020). Although the quantitative and qualitative changes of LDs or various vesicles according to the cell cycle are unclear, it is expected that these vesicles may also contribute to maintaining the density of the cytoplasm. In this respect, additional ODT-based studies on the physical properties and quantitative changes of vesicles according to the cell cycle may suggest new important clues in relation to previous studies.

Consequently, the hLD-SC, hUCM-MSC, and hiPSC stem cells can be distinguished from fibroblast cells based on the different physical properties (i.e., RI and volume distribution of organelle) of each stem cell (Fig. 5). Of note, the biological properties of the living cells cannot be distinguished using our method. Our approach, which non-invasively and quantitatively analyzes the physical properties of various organelles in live cells, could contribute to the elucidation of the characteristics and functions of various organelles distributed within stem cells.

Note: Supplementary information is available on the Molecules and Cells website (www.molcells.org).

ACKNOWLEDGMENTS

This work was supported by the National Research Foundation of Korea (NRF) through the Korean Ministry of Science & ICT (MSIT) (grant Nos., 2018R1D1A1B07048696, 2018R1A5A2020732, and 2019R1A2C2084122); the Korea Health Industry Development Institute (KHIDI), funded by the Ministry of Health & Welfare, Republic of Korea (grant No. HI18C2391); and a grant from the Asan Institute for Life Sciences, Asan Medical Center, Seoul, Korea (grant No. 2021IP0035-1). We would like to thank Tomocube Inc. for their technical support and discussion.

AUTHOR CONTRIBUTIONS

C.G.P. and J.K.K. conceptualized and acquired funding. Y.S., T.K.K., G.W.S., C.G.P., and Y.K. provided methodology and validation. Y.K., E.T., C.G.P., and J.K.K. wrote the draft manuscript. Y.K., C.G.P., and J.K.K. provided writing-review and editing. Y.M.O., C.G.P., and J.K.K. are supervised. All authors have read and agreed to the published version of the manuscript.

CONFLICT OF INTEREST

The authors have no potential conflicts of interest to disclose.

ORCID

Youngkyu Kim https://orcid.org/0000-0002-9595-1962
Tae-Keun Kim https://orcid.org/0000-0002-5533-5938
Yeonhee Shin https://orcid.org/0000-0001-8079-2922
Eunyoung Tak https://orcid.org/0000-0002-2595-3639
Gi-Won Song https://orcid.org/0000-0002-1581-7051
Yeon-Mok Oh https://orcid.org/0000-0003-0116-4683
Jun Ki Kim https://orcid.org/0000-0002-0099-9681
Chan-Gi Pack https://orcid.org/0000-0002-6578-3099

REFERENCES

Al-Bagdadi, F.A., Barona, H.M., Martinez-Ceballos, E., and Yao, S. (2019). Ultrastructure morphological characterization of different passages of rat dental follicle stem cells at in vitro culture. J. Microsc. Ultrastruct. *7*, 57-64.

Barer, R. (1953). Determination of dry mass, thickness, solid and water concentration in living cells. Nature *172*, 1097-1098.

Boulon, S., Westman, B.J., Hutten, S., Boisvert, F.M., and Lamond, A.I. (2010). The nucleolus under stress. Mol. Cell *40*, 216-227.

Choi, M., Ban, T., and Rhim, T. (2014). Therapeutic use of stem cell transplantation for cell replacement or cytoprotective effect of microvesicle released from mesenchymal stem cell. Mol. Cells *37*, 133-139.

Debnath, S.K. and Park, Y. (2011). Real-time quantitative phase imaging with a spatial phase-shifting algorithm. Opt. Lett. *36*, 4677-4679.

Gnutt, D., Gao, M., Brylski, O., Heyden, M., and Ebbinghaus, S. (2015). Excluded-volume effects in living cells. Angew. Chem. Int. Ed. Engl. *54*, 2548-2551.

Hantke, M.F., Hasse, D., Maia, F.R.N.C., Ekeberg, T., John, K., Svenda, M., Loh, N.D., Martin, A.V., Timneanu, N., Larsson, D.S.D., et al. (2014). High-throughput imaging of heterogeneous cell organelles with an X-ray laser. Nat. Photonics *8*, 943-949.

Herrera, M.B., Bruno, S., Buttiglieri, S., Tetta, C., Gatti, S., Deregibus, M.C., Bussolati, B., and Camussi, G. (2006). Isolation and characterization of a stem cell population from adult human liver. Stem Cells *24*, 2840-2850.

Johnsen, S. and Widder, E.A. (1999). The physical basis of transparency in biological tissue: ultrastructure and the minimization of light scattering. J. Theor. Biol. *199*, 181-198.

Jung, J., Kim, K., Yoon, J., and Park, Y. (2016). Hyperspectral optical diffraction tomography. Opt. Express *24*, 2006-2012.

Jung, M., Choi, H., Kim, J., and Mun, J.Y. (2020). Correlative light and transmission electron microscopy showed details of mitophagy by mitochondria quality control in propionic acid treated SH-SY5Y cell. Materials (Basel) *13*, 4336.

Kim, G., Lee, M., Youn, S., Lee, E., Kwon, D., Shin, J., Lee, S., Lee, Y.S., and Park, Y. (2018a). Measurements of three-dimensional refractive index tomography and membrane deformability of live erythrocytes from Pelophylax nigromaculatus. Sci. Rep. *8*, 9192.

Kim, K. and Guck, J. (2020). The relative densities of cytoplasm and nuclear compartments are robust against strong perturbation. Biophys. J. *119*, 1946-1957.

Kim, K., Lee, S., Yoon, J., Heo, J., Choi, C., and Park, Y. (2016b). Three-dimensional label-free imaging and quantification of lipid droplets in live hepatocytes. Sci. Rep. *6*, 36815.

Kim, K., Yoon, J., Shin, S., Lee, S., Yang, S.A., and Park, Y. (2016a). Optical diffraction tomography techniques for the study of cell pathophysiology. J. Biomed. Photonics Eng. *2*, 020201.

Kim, S., Lee, S., Kim, H., and Kim, T. (2018b). Exosomes secreted from induced pluripotent stem cell-derived mesenchymal stem cells accelerate skin cell proliferation. Int. J. Mol. Sci. *19*, 3119.

Kim, T.K., Lee, B.W., Fujii, F., Kim, J.K., and Pack, C.G. (2019a). Physico-chemical properties of nucleoli in live cells analyzed by label-free optical diffraction tomography. Cells *8*, 699.

Kim, T.K., Lee, B.W., Fujii, F., Lee, K.H., Lee, S., Park, Y., Kim, J.K., Lee, S.W., and Pack, C.G. (2019b). Mitotic chromosomes in live cells characterized using high-speed and label-free optical diffraction tomography. Cells *8*, 1368.

Kim, Y.S., Lee, S., Jung, J., Shin, S., Choi, H.G., Cha, G.H., Park, W., Lee, S., and Park, Y. (2018c). Combining three-dimensional quantitative phase imaging and fluorescence microscopy for the study of cell pathophysiology. Yale J. Biol. Med. *91*, 267-277.

Koster, A.J. and Klumperman, J. (2003). Electron microscopy in cell biology: integrating structure and function. Nat. Rev. Mol. Cell Biol. *Suppl*, SS6-SS10.

Lee, J., Choi, J., Kang, S., Kim, J., Lee, R., So, S., Yoon, Y.I., Kirchner, V.A., Song, G.W., Hwang, S., et al. (2020). Hepatogenic potential and liver regeneration effect of human liver-derived mesenchymal-like stem cells. Cells *9*, 1521.

Lee, J.H., Park, H.J., Kim, Y.A., Lee, D.H., Noh, J.K., Kwon, C.H.D., Jung, S.M., and Lee, S.K. (2012). The phenotypic characteristic of liver-derived stem cells from adult human deceased donor liver. Transplant. Proc. *44*, 1110-1112.

Lee, Y., Kim, T., Lee, M., So, S., Karagozlu, M.Z., Seo, G.H., Choi, I.H., Lee, P.C.W., Kim, C.J., Kang, E., et al. (2021). De novo development of mtDNA deletion due to decreased POLG and SSBP1 expression in humans. Genes (Basel) *12*, 284.

Li, J., Matlock, A., Li, Y., Chen, Q., Zuo, C., and Tian, L. (2019). High-speed in vitro intensity diffraction tomography. Adv. Photonics *1*, 066004.

Magidson, V. and Khodjakov, A. (2013). Circumventing photodamage in live-cell microscopy. Methods Cell Biol. *114*, 545-560.

Manos, P.D., Ratanasirintrawoot, S., Loewer, S., Daley, G.Q., and Schlaeger, T.M. (2011). Live-cell immunofluorescence staining of human pluripotent stem cells. Curr. Protoc. Stem Cell Biol. *19*, 1C.12.1-1C.12.14.

Najimi, M., Khuu, D.N., Lysy, P.A., Jazouli, N., Abarca, J., Sempoux, C., and Sokal, E.M. (2007). Adult-derived human liver mesenchymal-like cells as a potential progenitor reservoir of hepatocytes? Cell Transplant. *16*, 717-728.

Németh, A. and Grummt, I. (2018). Dynamic regulation of nucleolar architecture. Curr. Opin. Cell Biol. *52*, 105-111.

Pan, Q., Fouraschen, S.M.G., Kaya, F.S.F.A., Verstegen, M.M., Pescatori, M., Stubbs, A.P., van IJcken, W., van der Sloot, A., Smits, R., Kwekkeboom, J., et al. (2011). Mobilization of hepatic mesenchymal stem cells from human liver grafts. Liver Transpl. *17*, 596-609.

Park, C., Shin, S., and Park, Y. (2018). Generalized quantification of three-dimensional resolution in optical diffraction tomography using the projection of maximal spatial bandwidths. J. Opt. Soc. Am. A Opt. Image Sci. Vis. *35*, 1891-1898.

Park, Y., Diez-Silva, M., Fu, D., Popescu, G., Choi, W., Barman, I., Suresh, S., and Feld, M.S. (2010). Static and dynamic light scattering of healthy and malaria-parasite invaded red blood cells. J. Biomed. Opt. *15*, 020506.

Park, Y., Diez-Silva, M., Popescu, G., Lykotrafitis, G., Choi, W., Feld, M.S., and Suresh, S. (2008). Refractive index maps and membrane dynamics of human red blood cells parasitized by Plasmodium falciparum. Proc. Natl. Acad. Sci. U. S. A. *105*, 13730-13735.

Pepperkok, R. and Ellenberg, J. (2006). High-throughput fluorescence microscopy for systems biology. Nat. Rev. Mol. Cell Biol. *7*, 690-696.

Popescu, G., Park, Y., Lue, N., Best-Popescu, C., Deflores, L., Dasari, R.R., Feld, M.S., and Badizadegan, K. (2008). Optical imaging of cell mass and growth dynamics. Am. J. Physiol. Cell Physiol. *295*, C538-C544.

Sawyer, I.A., Sturgill, D., and Dundr, M. (2019). Membraneless nuclear organelles and the search for phases within phases. Wiley Interdiscip. Rev. RNA *10*, e1514.

So, S., Lee, Y., Choi, J., Kang, S., Lee, J.Y., Hwang, J., Shin, J., Dutton, J.R., Seo, E.J., Lee, B.H., et al. (2020). The Rho-associated kinase inhibitor fasudil can replace Y-27632 for use in human pluripotent stem cell research. PLoS One *15*, e0233057.

Stanly, T.A., Suman, R., Rani, G.F., O'Toole, P.J., Kaye, P.M., and Hitchcock, I.S. (2020). Quantitative optical diffraction tomography imaging of mouse platelets. Front. Physiol. *11*, 568087.

Takeda, M., Ina, H., and Kobayashi, S. (1982). Fourier-transform method of fringe-pattern analysis for computer-based topography and interferometry. J. Opt. Soc. Am. *72*, 156-160.

Wang, L.V. and Hu, S. (2012). Photoacoustic tomography: in vivo imaging from organelles to organs. Science *335*, 1458-1462.

Wolf, E. (1969). Three-dimensional structure determination of semi-transparent objects from holographic data. Opt. Commun. *1*, 153-156.

Woo, H.N., Park, S., Kim, H.L., Jung, M.K., Pack, C.G., Park, J., Cho, Y., Jo, D.G., Kim, D.K., Mook-Jung, I., et al. (2021). miR-351-5p/Miro2 axis contributes to hippocampal neural progenitor cell death via unbalanced mitochondrial fission. Mol. Ther. Nucleic Acids *23*, 643-656.

Yoon, J., Jo, Y., Kim, M., Kim, K., Lee, S., Kang, S.J., and Park, Y. (2017). Identification of non-activated lymphocytes using three-dimensional refractive index tomography and machine learning. Sci. Rep. *7*, 6654.

Zhu, H., Fan, J., Du, J., and Peng, X. (2016). Fluorescent probes for sensing and imaging within specific cellular organelles. Acc. Chem. Res. *49*, 2115-2126.